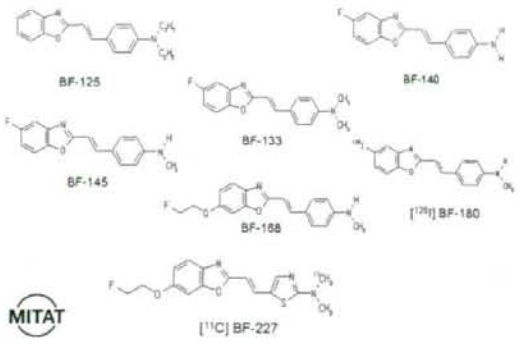

Figure 2. Chemical structures of our benzoxazole derivatives.

In Japan, our team has developed amyloid imaging probes since 1997 (Figure 2). We have previously reported a novel series of compounds including 6-(2-fluoroethoxy)-2-[2-(4-methylaminophenyl) ethenyl]-benzoxazole (BF-168), [2-(4-methylaminophenyl) ethenyl]-5-fluorobenzoxazole (BF-145) as promising candidates for *in vivo* imaging probes of SPs(11–13). These benzoxazole derivatives showed comparatively high permeability of blood-brain barrier (BBB), high affinity for Aβ aggregates, and high specificity for amyloid plaques including diffuse plaques, which suggests potential merit for detection of AD-related pathology. However, for application of these derivatives in a clinical PET study, we need to optimize the pharmacokinetic and safety of these molecules, and introduce an optimized derivative 2-[2-(2-dimethylaminothiazol-5-yl) ethenyl]-6-[2-(fluoro)ethoxy] benzoxazole (BF-227) as a candidate probe for *in vivo* imaging of amyloid in humans.

Material and methods

Affinity for synthetic Aβ1-42

Binding affinity of BF-227 for synthetic Aβ1-42 aggregates was examined as reported previously (12). Briefly, the binding assay was performed by mixing aliquot of aggregated Aβ1-42 with ^{125}I-labeled BF-180 (Figure 2).

Neuropathological staining in AD brain section

Postmortem brain tissues from autopsy-conformed AD cases were obtained from Fukushi-mura Hospital (Toyohashi, Japan). Experiments were performed under regulations of the ethics committee of the BF Research Institute. Brain sections were immersed in 100 μM of BF-227 solution containing 50 % ethanol.

BBB permeability of [^{11}C]BF-227 in normal mice

Brain uptakes of BF-227 were measured using ^{11}C-labeled compound. [^{11}C]BF-227 was administerd into the tail vein of normal mice. The mice were then sacrificed by decapitation at 2 and 60 min post injection (p.i.). The brains were removed and weighted, and the radioactivity was counted with an automatic γ-counter.

Acute and subacute toxicity of BF-227

Non-GLP toxicity study was carried out using female and male mice.

Other actions of BF-227

Postmortem brain section from autopsy-conformed AD cases was immersed in saline containing [^{11}C]BF-227, dipped in water, washed with EtOH, dried, and an autoradiographic image of the dried section was obtained using BAS-5000 phosphrimaging system (Fujifilm, Japan).

Ex vivo plaque labeling with BF-227 was evaluated using PS1/APPsw double transgenic mice. A BF-227 solution was administered into the tail vein.

Results

Affinity for synthetic Aβ1-42

The Ki value for Aβ1-42 fibrils in competitive binding assay using [^{125}I]BF-180 was 4.3 ± 1.3 nM in BF-227 (Kd value of [^{125}I]BF-180: 10.8 ± 1.5nM). This result suggests that BF-227 has a high binding affinity for Aβ1-42 fibrils.

Neuropathological staining in AD brain section

BF-227 clearly stained many SPs and diffuse plaques. This staining pattern corresponded to that of Aβ immunostaining in the adjacent section (Figure 3).

BBB permeability of [^{11}C]BF-227 in normal mice

Intravenous administration of [^{11}C]BF-227 into normal mice indicated that this labeled tracer readily penetrated the BBB (7.9 %ID/g at 2 min p.i.) and was washed out quickly (0.64 %ID/g at 60 min p.i.) from brain tissue.

Acute and subacute toxicity of BF-227

In an acute toxicity study, the lethal dose of BF-227 was larger than 10mg/kg (i.v.) for male and female

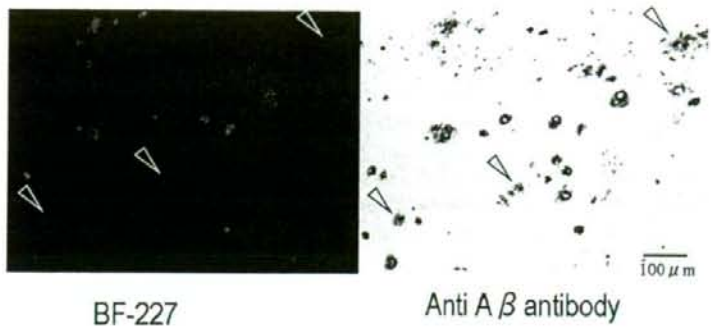

Figure 3. Neuropathological staining of amyloid plaques with BF-227 in AD brain sections. Sps and diffuse plaques (arrow head) were clearly stained with BF-227.

mice. In a subacute study, intravenous administration of BF-227 in tested doses did not produce any significant changes in general behavior and body weight. After 14 days post-treatment period, the mice did not show any microscopic alteration on pathological examination.

Other actions of BF-227

In the autoradiographic image using [^{11}C]BF-227, a specific binding pattern in the AD brain section was observed in the grey matter including SPs.

In the brain sections of PS1/APP Tg mice after intravenous injection of BF-227, numerous fluorescent spots were observed in the neocortex and hippocampus of the brain. These fluorescent spots corresponded to those of Aβ immunostaining in the same section.

Discussion and future prospects

BF-227 has high binding affinity to Aβ fibrils, remarkable stainability for SPs, high permeability of BBB, and fast clearance from normal brain tissue. The toxicity study of BF-227 indicates the sufficient safety margin of this compound for PET probe. Currently, we have investigated the clinical trial of [^{11}C]BF-227 in healthy subjects and in AD patients. This trial will elucidate the binding characteristics *in vivo* and the clinical usefulness of the probe in humans, and the results will be published by this summer or autumn.

Recently, we have introduced three novel compounds as candidate probes for *in vivo* imaging of tau pathology in the AD brain; 4-[2-(2-benzoimidazolyl) ethenyl]-N, N-diethylbenzenamine (BF-126), 2-[(4-methylamino) phenyl] quinoline (BF-158), and 2-(4-aminophenyl) quinoline (BF-170) (14) (Figure 4). In neuropathological examination,

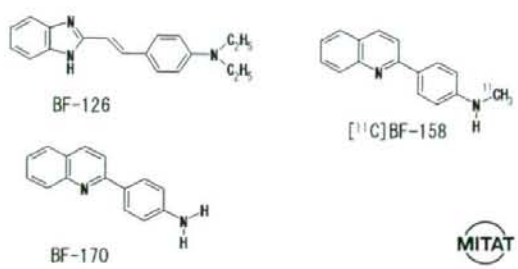

Figure 4. Chemical structures of our tau specific probes.

BF-126, BF-158, and BF-170 clearly stained NFTs, neuropil threads, and paired helical filament-type neuritis in the AD brain section. In addition, NFTs was labeled by 11C-labeled BF-158 with autoradiography. These findings suggest the potential usefulness of quinoline and benzimidazole derivatives for *in vivo* imaging of tau pathology in AD.

Several 11-C labeled probes for detecting SPs in AD patients have been reported from some teams. The short half-life (20 min) of 11-C, however, may limit the usefulness of these probes for a widespread application. Comparable 18-F labeled probes may supplant the clinical need due to the longer half-life of the isotope (109.7 min) (15). Further studies to develop 18-F labeled PET probes for the imaging of SPs are currently under way in some teams, including ours.

Unlike Alois Alzheimer, we now have access to instrumentation that allows visualization of the human brain *in vivo*. Brain imaging has become a part of the routine clinical assessment of dementia disorder (16). Recently, anti-amyloid agents such as Aβ vaccine and selective secretase inhibitors have been developed for the causal therapy of AD patients. AD patients all over the world may be

effectively diagnosed and treated by a combination of presymptomatic diagnosis and causal therapy.

Acknowledgement

The author thanks all the present and past members of our team and collaborators.

This study was financially supported by the Special Coordination Funds for Promoting Science and Technology, the Health and Labour Sciences Research Grants for Translational research from Ministry of Health, Labour and Welfare, Japan, the Program for Promotion of Fundamental Studies in Health Science of the National Institute of Biomedical Innovation, the New Energy and Industrial Technology Development Organization (NEDO), the Novartis foundation for Gerontological Research, the AstraZeneca Research Grant, and the Mitsui Sumitomo Insurance Welfare.

References

1. Shoji M, Golde TE, Ghiso J, Cheung TT, et al. Production of the Alzheimer amyloid beta protein by normal proteolytic processing. Science. 1992;258:126–9.
2. Lee VM, Balin BJ, Otvos L, Jr. Trojanowski JQ. A68: a major subunit of paired helical filaments and derivatized forms of normal Tau. Science. 1991;251:675–8.
3. Nordberg A. PET imaging of amyloid in Alzheimer's disease. Lancet Neurol. 2004;3:519–27.
4. Klunk WE, Debnath ML, Pettegrew JW. Chrysamine-G binding to Alzheimer and control brain: autopsy study of a new amyloid probe. Neurobiol Aging. 1995;16:541–8.
5. Skovronsky DM, Zhang B, Kung MP, Kung HF, et al. In vivo detection of amyloid plaques in a mouse model of Alzheimer's disease. Proc Natl Acad Sci U S A. 2000;97:7609–14.
6. Klunk WE, Bacskai BJ, Mathis CA, Kajdasz ST, et al. Imaging Abeta plaques in living transgenic mice with multiphoton microscopy and methoxy-X04, a systemically administered Congo red derivative. J Neuropathol Exp Neurol. 2002;61:797–805.
7. Shoghi-Jadid K, Small GW, Agdeppa ED, Kepe V, et al. Localization of neurofibrillary tangles and beta-amyloid plaques in the brains of living patients with Alzheimer disease. Am J Geriatr Psychiatry. 2002;10:24–35.
8. Klunk WE, Engler H, Nordberg A, Wang Y, et al. Imaging brain amyloid in Alzheimer's disease with Pittsburgh Compound-B. Ann Neurol. 2004;55:306–19.
9. Verhoeff NP, Wilson AA, Takeshita S, Trop L, et al. In-vivo imaging of Alzheimer disease beta-amyloid with [11C]SB-13 PET. Am J Geriatr Psychiatry. 2004;12:584–95.
10. Bacskai BJ, Klunk WE, Mathis CA, Hyman BT. Imaging amyloid-beta deposits in vivo. J Cereb Blood Flow Metab. 2002;22:1035–41.
11. Okamura N, Suemoto T, Shiomitsu T, Suzuki M, et al. A novel imaging probe for in vivo detection of neuritic and diffuse amyloid plaques in the brain. J Mol Neurosci. 2004;24:247–55.
12. Okamura N, Suemoto T, Shimadzu H, Suzuki M, et al. Styrylbenzoxazole derivatives for in vivo imaging of amyloid plaques in the brain. J Neurosci. 2004;24:2535–41.
13. Shimadzu H, Suemoto T, Suzuki M, Shiomitsu T, et al. Novel probes for imaging amyloid-beta: F-18 and C-11 labeling of 2-(4-aminostyryl)benzoxazole derivatives. Journal of Labelled Compounds & Radiopharmaceuticals. 2004;47:181–90.
14. Okamura N, Suemoto T, Furumoto S, Suzuki M, et al. Quinoline and benzimidazole derivatives: candidate probes for in vivo imaging of tau pathology in Alzheimer's disease. J Neurosci. 2005;25:10857–62.
15. Chandra R, Kung MP, Kung HF. Design, synthesis, and structure-activity relationship of novel thiophene derivatives for beta-amyloid plaque imaging. Bioorg Med Chem Lett. 2006;16:1350–2.
16. Nordberg A. Is amyloid plaque imaging the key to monitoring brain pathology of Alzheimer's disease in vivo? Eur J Nucl Med Mol Imaging. 2004;31:1540–3.

Journal of Neurochemistry, 2006, **99**, 198–205 doi:10.1111/j.1471-4159.2006.04035.x

Styrylbenzoazole derivatives for imaging of prion plaques and treatment of transmissible spongiform encephalopathies

Kensuke Ishikawa,* Yukitsuka Kudo,† Noriyuki Nishida,‡ Takahiro Suemoto,§ Tohru Sawada,§ Toru Iwaki¶ and Katsumi Doh-ura*

**Department of Prion Research, Tohoku University Graduate School of Medicine, Sendai, Japan*

†Division of Telecommunication and Information Technology, Biomedical Engineering Research Organization, Tohoku University, Sendai, Japan

‡Division of Cellular and Molecular Biology, Nagasaki University Graduate School of Biomedical Sciences, Nagasaki, Japan

§BF Research Institute Inc., Osaka, Japan

¶Department of Neuropathology, Graduate School of Medical Sciences, Kyushu University, Fukuoka, Japan

Abstract

Recent prevalence of acquired forms of transmissible spongiform encephalopathies (TSEs) has urged the development of early diagnostic measures as well as therapeutic interventions. To extend our previous findings on the value of amyloid imaging probes for these purposes, styrylbenzoazole derivatives with better permeability of blood–brain barrier (BBB) were developed and analyzed in this study. The new styrylbenzoazole compounds clearly labeled prion protein (PrP) plaques in brain specimens from human TSE in a manner irrespective of pathogen strain, and a representative compound BF-168 detected abnormal PrP aggregates in the brain of TSE-infected mice when the probe was injected intravenously. On the other hand, most of the compounds inhibited abnormal PrP formation in TSE-infected cells with IC_{50} values in the nanomolar range, indicating that they represent one of the most potent classes of inhibitor ever reported. BF-168 prolonged the lives of mice infected intracerebrally with TSE when the compound was given intravenously at the preclinical stage. The new compounds, however, failed to detect synaptic PrP deposition and to show pathogen-independent therapeutic efficacy, similar to the amyloid imaging probes we previously reported. The compounds were BBB permeable and non-toxic at doses for imaging and treatment; therefore, they are expected to be of practical use in human TSE.

Keywords: amyloid imaging, anti-prion activity, pathogen strain, prion disease, styrylbenzoazole derivatives.

J. Neurochem. (2006) **99**, 198–205.

The transmissible spongiform encephalopathies (TSEs) or prion diseases form a group of neurodegenerative disorders characterized by abnormal deposition of protease-resistant isoforms of prion protein (PrP) in the CNS (Prusiner 1991). TSEs are classified as sporadic, hereditary or environmentally acquired, and have become a serious public health issue because of the recent prevalence of acquired Creutzfeldt–Jakob disease (CJD), such as the variant form due to bovine spongiform encephalopathy (Will *et al.* 1996) and the iatrogenic form with cadaveric growth hormone or dura grafts (Brown *et al.* 2000). There is an urgent need to develop prophylactic and therapeutic interventions as well as diagnostic measures at the preclinical or early clinical stages of these incurable diseases.

We have previously reported that some amyloid imaging compounds, primarily derived from amyloid dyes such as

Received February 16, 2006; revised manuscript received May 25, 2006; accepted May 30, 2006.

Address correspondence and reprint requests to Dr Kensuke Ishikawa, Division of Prion Biology, Department of Prion Research, Tohoku University Graduate School of Medicine, 2–1 Seiryo-machi, Aoba-ku, Sendai 980-8575, Japan. E-mail: ishikawa@mail.tains.tohoku.ac.jp

Abbreviations used: AD, Alzheimer's disease; BBB, blood–brain barrier; BSB, (trans, trans)-1-bromo-2,5-bis-(3-hydroxycarbonyl-4-hydroxy)styrylbenzene; CJD, Creutzfeldt–Jakob disease; DMSO, dimethylsulfoxide; FDDNP, 2-(1-[6-[(2-fluoroethyl)(methyl)amino]-2-naphthyl]ethylidene)malononitrile; GSS, Gerstmann–Strässler–Scheinker syndrome; ICR, Institute of Cancer Research; ID, injected dose; NT, not tested; PrP, prion protein; PrPres, protease-resistant PrP; PTA, phosphotungstic acid; PVDF, polyvinylidene difluoride; TSE, transmissible spongiform encephalopathy.

Congo red and thioflavin T, are useful for detection of prion plaques and treatment of TSE (Ishikawa *et al.* 2004). These compounds, however, are limited in their ability because of inefficient brain uptake. Here we describe new compounds, styrylbenzoazole derivatives, which have been developed for practical use and analyzed for their PrP imaging ability, anti-prion activity, therapeutic efficacy, brain uptake and toxicity.

Materials and methods

Chemicals and experimental models

All of the test compounds were synthesized at Tanabe R & D (Saitama, Japan) and used freshly after being dissolved in 100% dimethylsulfoxide (DMSO).

Cultured cells were grown in Opti-MEM (Invitrogen, Carlsbad, CA, USA) supplemented with 10% fetal calf serum. As cellular models of TSE, we used mouse neuroblastoma (N2a) cells persistently infected with the RML strain (ScN2a) (Race *et al.* 1988) and six other prion-infected cell lines: N2a58 cells individually infected with the RML strain, the 22L strain (Nishida *et al.* 2000) and Fukuoka-1 strain (Ishikawa *et al.* 2004); N2a cells infected with the 22L strain; mouse hypothalamic cells (GT1-7) infected with the 22L strain (Milhavet *et al.* 2000); and mouse fibroblast cells (L929) infected with the RML strain (Vorberg *et al.* 2004).

Tg7 mice overexpressing hamster PrP (Race *et al.* 1995) and Tga20 mice overexpressing mouse PrP (Fischer *et al.* 1996) were also used. These mouse models were intracerebrally infected with 20 μL brain homogenate comprising 1% (w/v) of the 263K strain and the RML strain respectively. The Tg7 mice showed plaque-type PrP deposition between the cerebral cortex and hippocampus by 6 weeks after infection, followed by synaptic-type PrP deposition in the thalamus. The Tga20 mice showed similar pathological deposition, but plaques were not seen as frequently. Each mouse weighed ~30 g, and was maintained under deep ether anesthesia for minimum distress during all surgical procedures. Permission for the animal study was obtained from either the Animal Experiment Committee of Kyushu University or Tohoku University, Japan.

Brain uptake study

Test compounds were administered intravenously to Institute of Cancer Research (ICR) mice under ether anesthesia to determine initial brain uptakes. At 2 or 30 min after injection, the brains were removed, weighed and homogenized with saline. After centrifugation of the homogenate at 21 900 *g* for 10 min, the supernatant was applied to a conditioned C18 solid-phase extraction cartridge, and the compounds were eluted with methyl alcohol. Fluorescence was detected by high performance liquid chromatography with a fluorescence detector as reported previously (Okamura *et al.* 2005), and the percentage of injected dose per gram (%ID/g) was used as a measure of the level of the compounds in the brain.

In vitro PrP imaging in sections

Autopsy-diagnosed brain samples from cases of Gerstmann–Strässler–Scheinker syndrome (GSS) ($n = 2$), sporadic CJD ($n = 5$), iatrogenic dura CJD with synaptic PrP deposition ($n = 1$) and non-TSE control cases with amyloid lesions [Alzheimer's disease (AD), $n = 2$] or without amyloid lesions (cerebral infarction, $n = 1$) were obtained from the Department of Neuropathology, Kyushu University, Japan. After fixation in 10% buffered formalin for 2 weeks, each sample of TSE was immersed in 98% formic acid for the reduction of prion infectivity, embedded in paraffin and cut into sections 7 μm thick. Sections of a variant CJD case were kindly provided by Dr James W. Ironside of the CJD Surveillance Unit, Edinburgh, UK. For neuropathological staining, deparaffinized sections were immersed in 1% Sudan black solution to quench tissue autofluorescence. They were then incubated for 30 min in 1-μM solutions of the test compounds, rinsed with distilled water and examined under a fluorescence microscope (DMRXA; Leica Instruments, Wetzler, Germany) with a UV or FITC filter set.

For comparison, each section was subsequently immunoassayed for PrP as described previously (Doh-ura *et al.* 2000). Briefly, the sections were treated with a hydrolytic autoclave and incubated with a rabbit primary antibody, c-PrP, which was raised against a mouse PrP fragment, amino acids 214–228 (1 : 200; Immuno-Biological Laboratories, Gunma, Japan), followed by incubation with a horseradish peroxidase-conjugated secondary antibody (1 : 200; Vector Laboratories, Burlingame, CA, USA). The reaction product was developed with 3,3′-diaminobenzidine tetrahydrochloride solution and counterstained with hematoxylin. Paraffin-embedded brains of experimental animals were similarly investigated.

In vivo PrP imaging in model animals

BF-168 (molecular weight 312.34) dissolved in 10% DMSO was administered intravenously (0.5–5 mg/kg body weight) into Tg7 mice at 6–7 weeks after injection when the mice showed no apparent clinical signs of TSE. As controls, vehicle alone was similarly injected into infected mice, and BF-168 was administered into uninfected mice. The animals were killed at various time points, and the brains were rapidly frozen and cut into coronal sections 10 μm thick using a cryostat (CM3050; Leica Instruments). The sections were thaw-mounted on slides, dried and coverslipped. They were examined under a fluorescence microscope and further analyzed immunohistochemically as described above.

In vitro treatment in cell cultures

Abnormal PrP formation was assayed by the content of protease-resistant PrP (PrPres) in cellular models of TSE as described previously (Caughey and Raymond 1993). Each compound was added at the designated concentrations when cells were passaged at 10% confluence, while maintaining the final concentration of DMSO in the medium at < 0.5%. The cells were allowed to grow to confluence and lysed with lysis buffer (0.5% sodium deoxycholate, 0.5% Nonidet P-40, phosphate-buffered saline). For analysis of PrPres, samples were digested with 10 μg/mL proteinase K for 30 min, and the digestion was stopped with 0.5 mM phenylmethylsulfonyl fluoride. The samples were centrifuged at 100 000 *g* for 30 min, and pellets were resuspended in 1 × sample loading buffer and boiled. For analysis of cellular PrP in N2a cells, cell lysates were mixed directly with a quarter volume of 5 × sample loading buffer and boiled. These samples were separated by electrophoresis on a 15% Tris–glycine–sodium dodecyl sulfate polyacrylamide gel and electroblotted on to a polyvinylidene difluoride (PVDF) filter (Millipore, Bedford, MA, USA). PrP was detected using a monoclonal antibody, SAF83 (1 : 5000; SPI-BIO, Massy, France), followed by an alkaline phosphatase-conjugated

goat anti-mouse antibody (1 : 20 000; Promega, Madison, WI, USA). Immunoreactive blots were visualized with CDP-Star detection reagent (Amersham, Piscataway, NJ, USA). More than two independent assays were performed in each experiment and signals were analyzed using image analysis software. The approximate concentration of the compound giving 50% inhibition of PrPres formation, relative to the vehicle-treated control (IC_{50}), was estimated by signal intensity. To control for the detection limits of western blotting, we performed additional experiments utilizing sodium phosphotungstic acid (PTA) precipitation, which is the most sensitive technique presently available to detect PrPres (Safar *et al.* 1998). The PTA precipitation was undertaken on cell lysates of ScN2a treated with BF-168 at a designated concentration. The resulting pellets were collected by centrifugation and then analyzed by immunoblotting as described above.

In vivo treatment in model animals

BF-168 solution (4 mg/kg body weight) or vehicle alone was injected intravenously to experimental animals ($n = 5$) once a week. The treatment was started at 2 weeks after injection for Tg7 mice and at 4 weeks after injection for Tga20 mice, and repeated for 4 weeks. A continuous subcutaneous infusion of BF-168 was also given to Tga20 mice ($n = 5$) using an Alzet osmotic pump (Durect, Cupertino, CA, USA). In accordance with the manufacturer's instructions, each pump was filled with BF-168 solution at the designated doses and placed in a subcutaneous area of the back at 4 weeks after injection. The animals showed no apparent adverse effects of the treatment and were monitored 5 days a week until obvious clinical signs appeared. Statistical significance was analyzed by one-way ANOVA followed by Scheffé's method for multiple comparisons.

Results

Brain uptake and toxicity

We designed and synthesized novel styrylbenzoxazole derivatives (Table 1), styrylbenzothiazole and styrylbenzoimidazole derivatives (Table 2) with more efficient permeability of the BBB and less toxicity. Values for brain uptake at 2 min after intravenous injection of the compounds were in the 2.4–17.0%ID/g range, indicating a satisfactory level for imaging probes. Their washouts from the brain varied, with the ratio of %ID/g at 2 min to that at 30 min after injection ranging from 1.0 to 56.9. Acute toxicity was tested by administering each compound intravenously at ~10 mg/kg body weight into normal ICR mice. No apparent toxic effect was observed with any of the compounds tested.

PrP imaging ability

Imaging of abnormal PrP deposition by the compounds was first performed in brain sections of human TSE. The compounds fluorescently labeled most of the PrP plaques in cerebellar cortices of both GSS cases (Fig. 1a, representative data). Among sections from the sporadic CJD cases, PrP deposition was labeled only in a case with plaques (Fig. 1c). In the cerebral cortex from the variant CJD case, large core plaques were detectable, whereas the majority of immunopositive aggregates were not labeled (Fig. 1e). In contrast, no fluorescence signal was identified in sections from the dura CJD case or the other sporadic CJD cases that

Table1 Chemical structure, PrPres inhibition and brain uptake of styrylbenzoxazole derivatives including BF-168

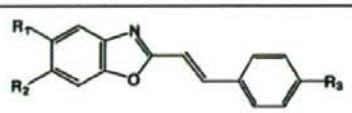

Compound	R_1	R_2	R_3	IC_{50} (nM)[a]	Brain uptake (%ID/g)[b] 2 min	Brain uptake (%ID/g)[b] 30 min	Ratio of 2 to 30 min brain uptake
BF-168	H	$O(CH_2)_2F$	$NH(CH_3)$	0.4	3.9[c]	1.6	2.4
BF-125	H	H	$N(C_2H_5)_2$	10.2	3.0	3.0	1.0
BF-133	F	H	$N(CH_3)_2$	1.6	5.5	3.8	1.4
BF-135	NO_2	H	$N(CH_3)_2$	< 1	NT[d]	NT	-
BF-140	F	H	NH2	< 1	5.5	1.1	5.0
BF-145	F	H	$NH(CH_3)$	< 1	4.4	1.6	2.8
BF-148	H	F	$N(CH_3)_2$	< 1	NT	NT	-
BF-165	H	H	$NH(CH_3)$	7.1	7.2	NT	-
BF-169	H	OH	$NH(CH_3)$	2.4	NT	NT	-
BF-173	I	H	NH_2	2.2	NT	NT	-
BF-180	I	H	$NH(CH_3)$	8.5	2.4	1.8	1.3
BF-191	H	H	Cl	1.8	12.0	1.7	7.1
BF-208	H	H	F	< 1	11.0	0.53	20.8
N-282	H	H	$N(CH_3)_2$	2.1	4.0	1.7	2.4
N-407	H	H	H	< 1	17.0	0.99	17.2

[a]IC_{50}, approximate concentration of a compound giving 50% inhibition of PrPres formation relative to the control in ScN2a cells.
[b]%ID/g, percentage of injected dose per gram in the brains of normal mice.
[c]already reported in the previous work (Okamura *et al.*, 2004).
[d]NT, not tested.

Table 2 Chemical structure, PrPres inhibition and brain uptake of styrylbenzothiazole and styrylbenzoimidazole derivatives

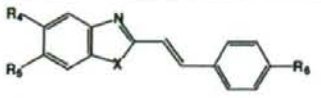

Compound	X	R_4	R_5	R_6	IC_{50} (nM)[a]	Brain uptake (%ID/g)[b] 2 min	Brain uptake (%ID/g)[b] 30 min	Ratio of 2 to 30min brain uptake
BF-124	S	H	H	$N(C_2H_5)_2$	18.1	2.4	2.5	1.0
BF-162	S	F	H	$N(CH_3)_2$	1.4	NT[c]	NT	-
N-276	S	H	H	$N(CH_3)_2$	< 1	NT	NT	-
N-438	S	H	H	H	< 1	11.0	2.0	5.5
BF-126	NH	H	H	$N(C_2H_5)_2$	21	7.2	0.16	45
BF-166	NH	F	H	$N(C_2H_5)_2$	1.1	NT	NT	-
N-457	NH	H	H	Cl	< 1	7.1	0.21	33.8
N-491	NH	H	H	H	1.9	7.4	0.13	56.9

[a]IC_{50}, approximate concentration of a compound giving 50% inhibition of PrPres formation relative to the control in ScN2a cells.
[b]%ID/g, percentage of injected dose per gram in the brains of normal mice.
[c]NT, not tested.

included perivacuolar and/or synaptic PrP deposition (data not shown). Background staining was barely observed after rinsing off the excess compound. Immunohistochemical analysis of PrP revealed that the compounds achieved high-specificity labeling (Figs 1b, d and f). The compounds displayed no signal in control sections without amyloid lesions (data not shown).

Similar results were observed in experimental mice. PrP plaques were specifically labeled in brain sections of Tg7 mice infected with the 263K strain, and there was no PrP immunopositive reaction or fluorescence signal in brain sections of uninfected mice (data not shown). We performed *in vivo* experiments using presymptomatic Tg7 mice at a later stage of TSE. A typical image is shown in Fig. 1(g); peripheral administration of BF-168 fluorescently labeled plaques in the cerebral white matter, indicating that the compound efficiently entered the brain and bound to coarse PrP deposits. Subsequent immunostaining verified the specificity and sensitivity for PrP (Fig. 1h). Non-specific staining, such as cerebrovascular labeling, was occasionally observed at 4 h after injection of 5 mg/kg BF-168, but not after 8 h or more. The stability of the fluorescence signals was examined at various time points up to 24 h after injection and the dye–PrP complex remained visible at the latest time. In contrast, there was no significant labeling after an injection of BF-168 into uninfected animals, or after an injection of vehicle alone to terminally ill Tg7 mice. Similar results were obtained for Tga20 mice infected with the RML strain, although plaques were less frequently detected (data not shown).

Anti-prion activity *in vitro*

The anti-prion activities of the compounds were investigated using ScN2a cells, which are most commonly used for drug screening for TSE treatment. Styrylbenzoxazole derivatives, including BF-168, were evaluated and confirmed to inhibit PrPres formation with IC_{50} values in the nanomolar or subnanomolar range (Fig. 2a and Table 1). Styrylbenzothiazole and styrylbenzoimidazole derivatives were similarly potent, in a dose-dependent manner, within a non-toxic dose range (~10 μM) (Table 2). Treatment with vehicle alone showed no inhibitory effect compared with untreated controls (Fig. 2a). We utilized PTA precipitation, which increases the sensitivity of western blotting, and confirmed the potency of BF-168 at a concentration of 10 times the IC_{50}. Furthermore, radiographic film was exposed to the blotted PVDF membranes for 10 times longer than usual before developing. No significant signals were visualized, whereas bands representing the vehicle-treated control were so strong as to be already saturated (Fig. 2b). To determine whether the efficacy was transient, ScN2a cells treated with 10 nM BF-168 were further cultured for 2 weeks in the absence of BF-168. PrPres signals never reappeared, even through four passages after discontinuation of the treatment (Fig. 2c). To exclude the possibility of interference with immunodetection, BF-168 solution at a final concentration of 10 nM was added to a lysate of untreated ScN2a cells before proteinase K digestion. PrP signals were not affected (data not shown). Nor was any alteration observed in cellular PrP level of N2a cells after treatment with 10 nM BF-168 (Fig. 2d).

To investigate whether the efficacy of the compounds depends on pathogen strain, we tested BF-168 in three N2a58 cell lines individually infected with different strains. As shown in Table 3, BF-168 was only effective in N2a58 cells infected with the RML strain, although the inhibitory activity was not as strong as in ScN2a cells (~1 μM). In contrast, BF-168 was ineffective in the same N2a58 cells infected with the 22L or Fukuoka-1 strains up to 10 μM, a dose at which the compound showed host cytotoxicity.

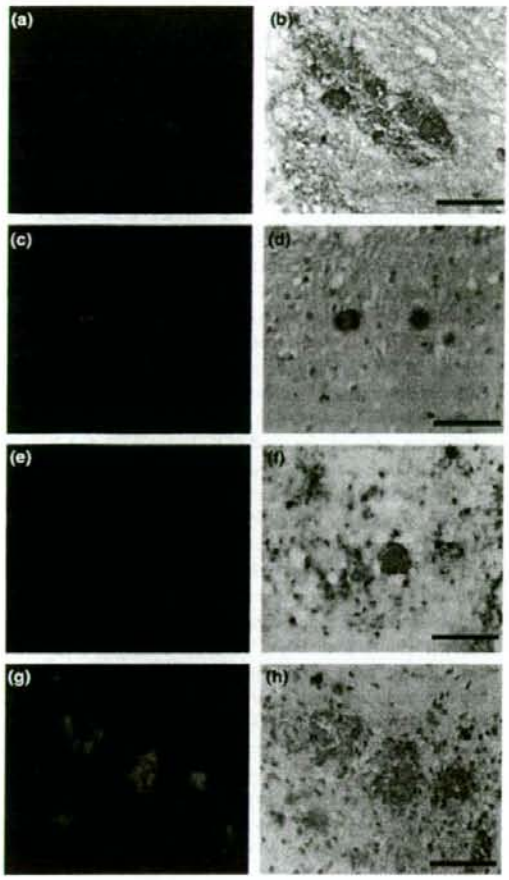

Fig. 1 PrP imaging *in vitro* and *in vivo*. BF-168 fluorescently labeled PrP deposition in a cerebellar section from the case of GSS (a), and in cerebral sections from cases of sporadic CJD with plaques (c) and variant CJD (e). Similar results were obtained from the brains of living TSE-infected mice that were intravenously injected with BF-168 solution (0.5 mg/kg). BF-168 detected PrP deposition in the cerebral white matter between the cortex and hippocampus (g). Sections (a, c, e and g) were subsequently immunoassayed for PrP (b, d, f and h). Bars represent 100 μm (a–f) and 25 μm (g and h).

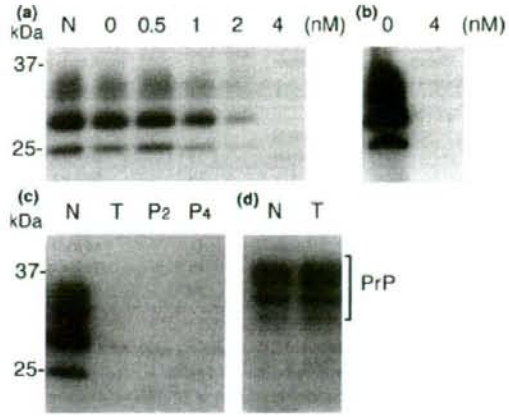

Fig. 2 Effects of BF-168 on PrP expression in ScN2a and N2a cells. BF-168 was added at the designated concentrations to freshly passaged cells. PrPres formation in ScN2a cells was inhibited in a dose-dependent manner (a). To exclude the sensitivity limit of immunoblotting, ScN2a cells treated with 4 nM BF-168 were also analyzed by sodium PTA, and no significant signals were visualized (b). ScN2a cells treated with 10 nM BF-168 were maintained for an additional four passages, and the PrPres signal was not restored in the absence of BF-168 (c). PrP expression was not affected in N2a cells that were grown in the presence of 10 nM BF-168 (d). Lane N, untreated cells; lane 0, cells treated with vehicle alone; lane T, cells treated with 10 nM BF-168; lanes P_2 and P_4, cells following two and four passages after treatment respectively. Bars on the left indicate molecular size markers at 37 and 25 kDa.

Table 3 Anti-prion activities (IC_{50}) of BF-168 in various types of TSE-infected cells

Host cells	Pathogen strains		
	RML	22L	Fukuoka-1
N2a	0.4 nM	None[a]	-[b]
N2a58	~ 1 μM	None	None
L929	~ 10 nM	-	-
GT1-7	-	None	-

[a]None, no significant PrPres inhibition up to 10 μM, a dose that affect the rate of cell growth.
[b], not available.

Furthermore, we established L929 cells stably infected with the RML strain. BF-168 inhibited PrPres formation in the RML-infected L929 cells with an IC_{50} in the nanomolar range. We also tested potency against the 22L strain in two other cell lines, N2a and GT1-7 cells. BF-168 was ineffective in either cell line infected with the 22L strain. Other compounds tested here demonstrated similar results (data not shown). These results suggest that the styrylbenzoxazole derivatives exert their inhibitory activity on PrPres formation in a strain-dependent, but not a host cell-dependent, manner.

Therapeutic efficacy *in vivo*

The therapeutic activity of the compounds *in vivo* was assayed in two different mouse models using BF-168 as a representative. Treatment was initiated 2–4 weeks after TSE infection and repeated once a week for 4 weeks. The dosage at a single administration corresponded to a dose sufficient to detect PrP plaques. As shown in Table 4, there was no

Table 4 Effects of BF-168 treatment on intracerebrally TSE-infected mice

Mouse - pathogen strain	*n*	Dose (mg/kg/week)	Administration	Incubation period Mean ± SD (days)
Tg7 - 263K				
	7	Control	-	49.4 ± 1.9
	5	Vehicle	i.v.[a]	50.2 ± 4.1
	5	4	i.v.	52.2 ± 2.6
Tga20 - RML				
	7	Control	-	66.6 ± 1.6
	5	Vehicle	i.v.	64.8 ± 1.6
	5	4	i.v.	72.2 ± 2.5*
	5	10	s.c.[b]	66.0 ± 3.1

* $p < 0.001$ versus the oher groups.

[a]i.V., intravenous injection of BF-168 once a week for 4 weeks from 2 weeks p.i. for Tg7, or 4 weeks p.i. for Tga20.

[b]s.c., continous subcutaneous infusion of BF-168 for 4 weeks from 4 weeks p.i.

significant difference in incubation periods between groups of Tg7 mice infected intracerebrally with the 263K strain, with or without treatment. In contrast, intravenous injection with 4 mg/kg BF-168 significantly prolonged the incubation period (~ 11.4%) of Tga20 mice intracerebrally infected with the RML strain.

In another trial, we used osmotic pumps filled with BF-168 solution, assuming that the route of administration is a key issue. The pump worked continuously for 4 weeks, and the total dosage for the duration was selected to correspond to two to three times that administered intravenously. Subcutaneous infusion of BF-168, however, did not prolong incubation periods of Tga20 mice intracerebrally infected with the RML strain (Table 4). There was no significant difference in incubation period in either group of infected mice between untreated controls and controls treated with vehicle alone.

Discussion

Our results show that styrylbenzoazole derivatives represent candidates for imaging probes as well as therapeutic drugs for TSE. It has been increasingly necessary to develop minimally non-invasive methods for recognizing early clinical infection and evaluating treatment of TSE. We have already focused on two β-amyloid imaging probes and reported them as potential agents for TSE (Ishikawa *et al.* 2004). The problem is, however, that they seemed to have practical limitations because of inadequate brain uptake and washout. Here, we confirmed that novel styrylbenzoazole derivatives clearly labeled PrP plaques *in vitro* and BF-168, the parent compound, entered the brain and labeled PrP plaques *in vivo*, even at a 20-fold lower dose than the probes we previously reported. In brain uptake studies, all of the compounds showed BBB permeability with >1%ID/g, which is proposed to be sufficient for neuroimaging probes. The background staining of 0.5 mg/kg BF-168 was almost absent at 4 h after administration, suggesting excellent clearance from the brain.

Most of styrylbenzoazole derivatives labeled β-amyloid aggregates in AD specimens in this study (data not shown) as well as in the previous study on Alzheimer's (Okamura *et al.* 2004). This is also observed with 2-(1-[6-[(2-fluoroethyl)(methyl)amino]-2-naphthyl]ethylidene)malononitrile (FDDNP), one of the promising agents for imaging β-amyloid deposition. FDDNP has been reported to label PrP plaques in brain sections, and is a candidate for imaging PrP deposition (Bresjanac *et al.* 2003). These findings imply lack of disease specificity, but the compounds should still be useful for some types of TSE, because anatomical distributions of amyloid deposition are characteristically different between diseases. Pathological changes including amyloid deposition of AD brain are always observed in the hippocampus but not in the cerebellum, whereas those of TSE tend to be absent from the hippocampus but to be demonstrated in the cerebellum.

Styrylbenzoazole derivatives detected predominantly PrP plaques, especially in specimens of sporadic CJD with plaques and variant CJD. However, their ability to detect synaptic or perivacuolar PrP deposition remains inconclusive, until more sensitive investigations, such as autoradiography, are available. The compounds tested in this study can be used with radionuclides. ^{18}F-radiolabeled BF-168, which has already been employed for labeling of β-amyloid deposits including both neuritic and diffuse plaques in AD brain (Okamura *et al.* 2004), may be a suitable tool for investigating whether PrP deposition, other than plaque type, can be detected.

This study demonstrated that styrylbenzoazole derivatives have more potent anti-prion activity than the amyloid imaging probes reported previously (Ishikawa *et al.* 2004). Although the neuropathological processes remain unclear, one of the most likely strategies for TSE treatment is a small-molecule drug that can enter the brain and inhibit abnormal PrP formation. It is important to emphasize that styrylbenzoazole derivatives have a wide concentration safety margin, and some were effective even at subnanomolar doses in ScN2a cells. Dozens of drug candidates for TSE have been reported to date but, as far as we know, the most potent inhibitor class for abnormal PrP formation in ScN2a cells is specific blocking antibodies with an IC_{50} in the nanomolar range (Peretz *et al.* 2001).

BF-168 showed no apparent alteration in cellular PrP expression level in N2a cells, and also labeled abnormal PrP deposition both *in vitro* and *in vivo*. These data suggest that styrylbenzoazole derivatives might interact directly with abnormal PrP molecules to block the conversion of normal to abnormal PrP. The structure–activity relationship, examined by introducing side-chain or functional groups into the benzoazole and/or benzene rings, demonstrates that the inhibitory potency is not always the same, even among

closely related compounds (data not shown). Although we could not obtain any insight into inhibitory mechanisms, the efficacy of BF-168 was dependent on pathogen strain, and this is consistent with our previous work using three types of cell lines (Ishikawa *et al.* 2004). In an attempt to further explore strain dependency, we tested three different pathogen strains in one host cell line, and three different host cell lines with one pathogen strain. BF-168 inhibited abnormal PrP formation in all three types of RML-infected cells, including ScN2a cells. By contrast, BF-168 did not demonstrate any inhibitory activity in the 22L- or Fukuoka-1-infected cells. It is well known that prion strains differ in their biological profiles such as the degree of glycosylation and the conformation of PrP molecules. In the imaging experiments we confirmed that the compound bound to a certain type of abnormal PrP aggregates. Thus, it was assumed that the therapeutic efficacy might be based on blocking certain interactions between normal and abnormal PrP, and that BF-168 might recognize the PrP conformation. However, considering a discrepancy in the *in vivo* experiment between PrP imaging and treatment using infected Tg7 mice, these inferences remain unsupported and the precise mechanism of the strain-dependent efficacies needs to be elucidated.

Kocisko *et al.* (2004) reported that anti-prion activity *in vitro* does not always correlate with that *in vivo*. With *in vivo* testing, there are many variables, such as inoculation route, dosing protocol and pathogen strain. The efficacy differed according to the BF-168 administration route in Tga20 mice, even though the dose administered subcutaneously for the same duration was no less than that administered intravenously. This might be due to differences in stability and clearance of BF-168 in relation to the route of administration.

Most previous therapeutic investigations showed a significant benefit *in vivo* when the treatment was started before, or soon after, peripheral TSE infection. Although the efficacy of BF-168 was limited, it is noteworthy that we obtained significant results with peripheral administration at a later stage of the intracerebral infection. In addition, BF-168 showed excellent brain uptake and binding affinity towards PrP aggregates *in vivo*, even at a low dose, suggesting that the compound should be a good imaging probe for clinical use. In the treatment of infected Tga20 mice, BF-168 showed almost the same prolongation of the incubation period but with a 10-fold smaller dose than (trans, trans)-1-bromo-2,5-bis-(3-hydroxycarbonyl-4-hydroxy)styrylbenzene (BSB), which we reported previously as one of the amyloid imaging probes applicable for TSE (Ishikawa *et al.* 2004). BF-168 showed a low IC_{50} of 0.4 nM in treatment of ScN2a cells, whereas the IC_{50} of BSB was more than 1000-fold higher (1.4 μM). We decided the dosing protocol for our experimental animals from *in vitro* data, including the ratio of these IC_{50} values, and from an *invivo* imaging experiment in which 0.1 mg BF-168 per injection was enough to detect PrP deposition. It is also necessary to consider washout of the compound from the brain. Further studies are required to examine issues such as dose–response relationships, administration time and dosing conditions. Furthermore, there was a problem in that administration frequency was limited because animal tail tissue was damaged by repetitive intravenous injections. In addition, it should be investigated whether compounds with slower washout from the brain are more suitable as therapeutic agents.

In conclusion, styrylbenzoazole derivatives efficiently entered the brain and labeled pathological PrP deposition, and demonstrated some anti-prion activities both *in vitro* and *in vivo*. Although their efficacy depended on the pathogen strain, these are a new class of compounds with potential as therapeutic drugs and imaging probes for TSE.

Acknowledgements

This study was supported by grants to KD from the Ministry of Health, Labour and Welfare (H16-kokoro-024) and the Ministry of Education, Culture, Sports, Science and Technology 13557118, 14021085, Japan. The authors thank Dr James W. Ironside of the CJD Surveillance Unit, Edinburgh, UK, for providing the variant CJD specimens.

References

Bresjanac M., Smid L. M., Vovko T. D., Petric A., Barrio J. R. and Popovic M. (2003) Molecular-imaging probe 2-(1-[6-[(2-fluoro-ethyl)(methyl) amino]-2-naphthyl]ethylidene) malononitrile labels prion plaques *in vitro*. *J. Neurosci.* **23**, 8029–8033.

Brown P., Preece M., Brandel J. P. *et al.* (2000) Iatrogenic Creutzfeldt–Jakob disease at the millennium. *Neurology* **55**, 1075–1081.

Caughey B. and Raymond G. J. (1993) Sulfated polyanion inhibition of scrapie-associated PrP accumulation in cultured cells. *J. Virol.* **67**, 643–650.

Doh-ura K., Mekada E., Ogomori K. and Iwaki T. (2000) Enhanced CD9 expression in the mouse and human brains infected with transmissible spongiform encephalopathies. *J. Neuropathol. Exp. Neurol.* **59**, 774–785.

Fischer M., Rulicke T., Raeber A., Sailer A., Moser M., Oesch B., Brandner S., Aguzzi A. and Weissmann C. (1996) Prion protein (PrP) with amino-proximal deletions restoring susceptibility of PrP knockout mice to scrapie. *EMBO J.* **15**, 1255–1264.

Ishikawa K., Doh-ura K., Kudo Y., Nishida N., Murakami-Kubo I., Ando Y., Sawada T. and Iwaki T. (2004) Amyloid imaging probes are useful for detection of prion plaques and treatment of transmissible spongiform encephalopathies. *J. Gen. Virol.* **85**, 1785–1790.

Kocisko D. A., Morrey J. D., Race R. E., Chen J. and Caughey B. (2004) Evaluation of new cell culture inhibitors of protease-resistant prion protein against scrapie infection in mice. *J. Gen. Virol.* **85**, 2479–2483.

Milhavet O., McMahon H. E., Rachidi W. *et al.* (2000) Prion infection impairs the cellular response to oxidative stress. *Proc. Natl Acad. Sci. USA* **97**, 13 937–13 942.

Nishida N., Harris D. A., Vilette D., Laude H., Frobert Y., Grassi J., Casanova D., Milhavet O. and Lehmann S. (2000) Successful transmission of three mouse-adapted scrapie strains to murine neuroblastoma cell lines overexpressing wild-type mouse prion protein. *J. Virol.* **74**, 320–325.

Okamura N., Suemoto T., Shimadzu H. *et al.* (2004) Styrylbenzoxazole derivatives for *in vivo* imaging of amyloid plaques in the brain. *J. Neurosci.* **24**, 2535–2541.

Okamura N., Suemoto T., Furumoto S. *et al.* (2005) Quinoline and benzimidazole derivatives: candidate probes for *in vivo* imaging of tau pathology in Alzheimer's disease. *J. Neurosci.* **25**, 10 857–10 862.

Peretz D., Williamson R. A., Kaneko K. *et al.* (2001) Antibodies inhibit prion propagation and clear cell cultures of prion infectivity. *Nature* **412**, 739–743.

Prusiner S. B. (1991) Molecular biology of prion diseases. *Science* **252**, 1515–1522.

Race R. E., Caughey B., Graham K., Ernst D. and Chesebro B. (1988) Analyses of frequency of infection, specific infectivity, and prion protein biosynthesis in scrapie-infected neuroblastoma cell clones. *J. Virol.* **62**, 2845–2849.

Race R. E., Priola S. A., Bessen R. A., Ernst D., Dockter J., Rall G. F., Mucke L., Chesebro B. and Oldstone M. B. (1995) Neuron-specific expression of a hamster prion protein minigene in transgenic mice induces susceptibility to hamster scrapie agent. *Neuron* **15**, 1183–1191.

Safar J., Wille H., Itri V., Groth D., Serban H., Torchia M., Cohen F. E. and Prusiner S. B. (1998) Eight prion strains have PrP(Sc) molecules with different conformations. *Nat. Med.* **4**, 1157–1165.

Vorberg I., Raines A., Story B. and Priola S. A. (2004) Susceptibility of common fibroblast cell lines to transmissible spongiform encephalopathy agents. *J. Infect. Dis.* **189**, 431–439.

Will R. G., Ironside J. W., Zeidler M. *et al.* (1996) A new variant of Creutzfeldt–Jakob disease in the UK. *Lancet* **347**, 921–925.

III. 臨 床 編

アルツハイマー病の診断 新しい診断法の開発 アミロイドイメージング PET

In vivo amyloid imaging using PET

岡村信行[1] 谷内一彦[1] 古川勝敏[2] 荒井啓行[2] 工藤幸司[3]

Key words：アルツハイマー病，老人斑，アミロイドβ蛋白，positron emission tomography(PET)

はじめに

認知症の診断プロセスにおいて，脳内の器質性変化を正確に把握することは重要であり，その手段としての画像診断の役割は大きい．従来の画像診断では，萎縮や血流・代謝の低下を認知症診断の指標としてきた．これらは主として神経細胞の脱落を反映した変化である．軽度認知機能障害(MCI)以降の症状が顕在化した段階での診断には優れた指標となるが[1]，神経細胞の脱落が軽微な段階では，その検出力に限界がある．

アルツハイマー病(AD)では，神経細胞の脱落に先立って，アミロイドβ蛋白，タウ蛋白を主要構成成分とする老人斑，神経原線維変化の脳内沈着が出現する[2]．これらは同時に疾患特異性の高い変化でもある．したがって，上記病理像を生体で非侵襲的に検出し得る検査こそが，ADを早期診断するうえで理想的な診断法となる．こうした理由から，アミロイドの脳内蓄積を非侵襲的に計測する画像診断法(アミロイドイメージング)が近年脚光を浴びるようになった．ここ数年の研究の進展により，ADの早期診断におけるアミロイドイメージングの有用性が広く認知された．更に，MCIあるいは無症候段階における進行予測や，脳内のアミロイドβ蛋白蓄積量をモニタリングする新たな薬効評価系としても，その活用が強く期待されている．

そこで本稿では，近年進歩の著しいpositron emission tomography(PET)を用いたアミロイドイメージングについて紹介する．

1. アミロイドイメージング用プローブ

PETを用いてアミロイドを画像化するには，アミロイドのβシート構造に結合親和性を有する低分子化合物をポジトロン放出核種(^{11}Cあるいは^{18}F)で標識し，これをプローブとして用いる[3]．静脈から投与されたプローブが脳内へ移行し，老人斑に選択的に結合して局所からの排出が遅延する性質を利用して，プローブの結合した老人斑の脳内濃度を計測する．これまでに，[^{18}F]FDDNP，[^{11}C]PIB，[^{11}C]SB-13，[^{11}C]BF-227などの複数のアミロイドイメージング用プローブが臨床応用されている．プローブの開発状況の詳細については本誌の工藤らの別稿を参照されたい．本稿ではPIBとBF-227

[1]Nobuyuki Okamura, Kazuhiko Yanai: Department of Pharmacology, Tohoku University School of Medicine 東北大学大学院医学系研究科 機能薬理学分野 [2]Katsutoshi Furukawa, Hiroyuki Arai: Department of Geriatrics and Gerontology 同 老年病態学分野 [3]Yukitsuka Kudo: Tohoku University Biomedical Engineering Research Organization(TUBERO) 東北大学先進医工学研究機構

0047-1852/08/¥40/頁/JCLS

のPET所見を中心に述べる．

2. PIB

a. アルツハイマー病早期診断への応用

現在最も多くの施設で利用されているプローブは，^{11}Cで標識されたPIB(正式名6OH-BTA-1)である．母化合物であるthioflavin Tと同様にAD脳内に蓄積した老人斑に選択的に結合する特性に加えて，高い脳血液関門透過性を有する[4]．このPIBを用いてAD患者でPET検査を実施すると，大脳皮質領域を中心にPIBの顕著な集積が観察され，その集積分布はBraak and Braakが記載した老人斑の蓄積分布に一致する[5,6]．更にMCIの約半数の症例でもAD患者と同様の高集積が観察される[6,7]．これらの症例は既に老人斑の沈着が進行し，ADと同等の病理像を呈した'AD発症予備群'と推測される．実際にMCIでPIB高集積を示した症例の多くがADに進行したとのpreliminaryな報告もあり，PIB-PETでMCIの予後予測ができる可能性は高い．

b. 非アルツハイマー型変性認知症での所見

PIBの異常集積を示す疾患はADには限定されず，レビー小体型認知症(DLB)の多くの症例でも集積上昇を認める．ただし，この集積上昇がレビー小体の沈着を反映しているとは考えにくい．*in vitro*での検討では，PIBのαシヌクレインとの結合性はAβに比して低いとされている[8]．DLBにおけるPIBの集積分布はAD患者とほぼ共通しているため，むしろ併存するAβ蓄積病変を反映した変化と考えられる[6]．一方，前頭側頭葉型認知症(FTD)などのタウオパチーでは正常な集積像を示し，ADとの鑑別に有用である．またPIBは神経原線維変化への結合性も低く[8]，辺縁系への神経原線維変化の蓄積を主体とする認知症の検出力は低いと予想される．

c. 発症前診断への応用は可能か

アミロイドイメージングに課された役割として，無症候例での老人斑沈着が検出可能か否かに注目が集まる．41人の認知機能正常例を対象とした検討[9]では，うち4人でPIBの高集積が認められている．同症例では脳脊髄液中Aβ42濃度の低下も併せて観察されており[10]，症状発現前の老人斑沈着を反映している可能性が高い．このような集積が，良性(正常加齢の範囲内)のものか，悪性(ADへの進行を示唆する老人斑の病的沈着)のものかを見極めることは現時点では難しい．今後，PET検査実施例を長期にフォローアップすることにより，結論が下される．

もう1点検証する必要があるのは，PET画像が老人斑の蓄積分布を本当に忠実に反映しているか否かという点である．これには病理と画像の対比研究が求められよう．最近PIB-PETを施行した症例の剖検結果が報告されている[11]．この症例は，DLBの臨床診断でありながら，生前のPET検査ではPIBの高集積が認められていた．病理でもDLBの診断が下されたが，Aβの病理としては脳アミロイドアンギオパチーが顕著であった．老人斑の沈着はびまん性老人斑を主体とした軽微な変化にとどまっており，本症例では脳血管アミロイドの存在がPIBの集積に大きく関与していると考えられる．したがって，アミロイドイメージングにおける異常集積例に対しては，老人斑以外へのプローブの結合の可能性も念頭に置いた慎重な解釈が求められる．

3. BF-227

著者らはベンズオキサゾール誘導体がアミロイドイメージング用プローブの候補化合物になり得ることを見いだし[12]，その最適化化合物であるBF-227の臨床的有用性を検証している．[^{11}C]BF-227投与後20-40分のPET画像を観察すると，AD患者では大脳皮質領域で[^{11}C]BF-227の顕著な集積が確認できる(**図1-a**)．側頭葉におけるSUV対小脳比を算出すると，AD患者のほぼ全例で高値を示し，診断に有用である[13]．更にSPM2ソフトウェアを用いて，健常者に比べてAD患者で有意な集積上昇のみられた脳領域を抽出した結果，側頭-頭頂葉領域を中心とする大脳皮質の広範な領域で集積上昇が確認された(**図1-b**)．このような集積分布は，病理学的研究で示されているneuritic plaqueの

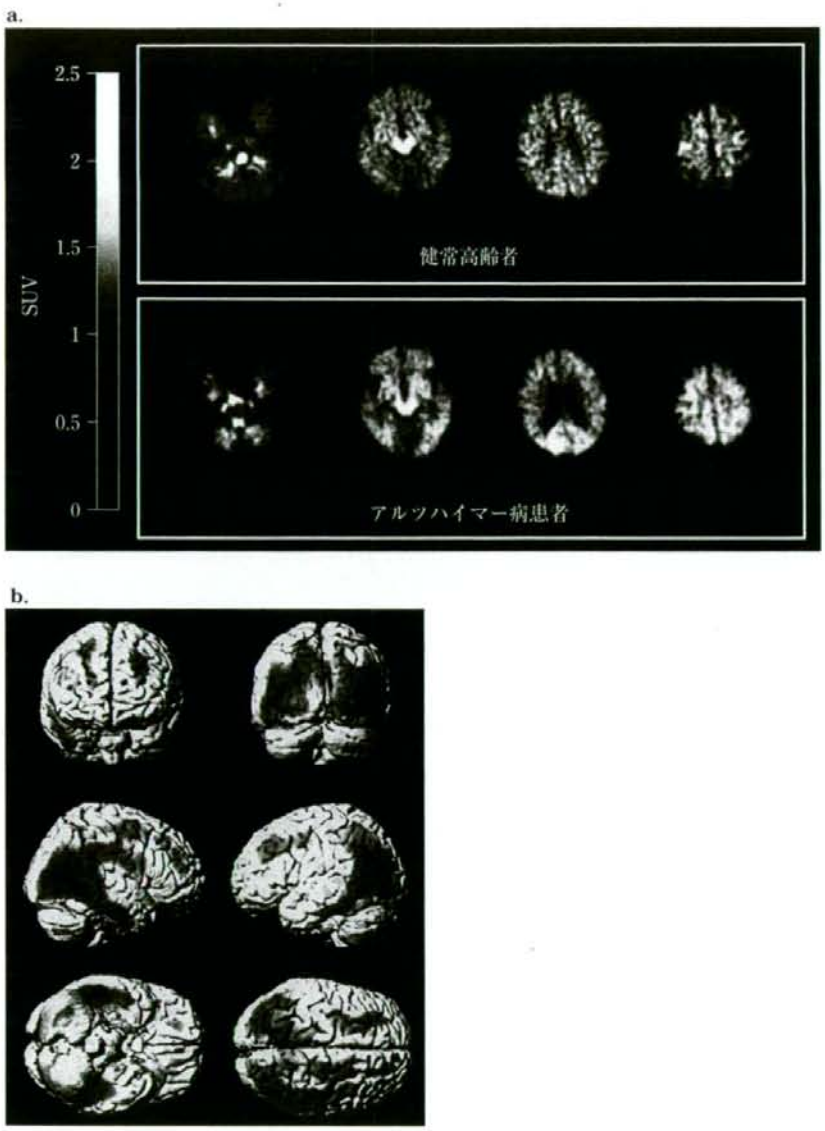

図1 [^{11}C]BF-227投与後20-40分のPET画像(a)，アルツハイマー病患者での集積上昇部位(b)

沈着分布に近く，比較的成熟した老人斑の蓄積を反映しているものと推測される．

MCIでは，PIBと同様，半数以上の症例で大脳皮質領域での集積上昇が観察されているが，健常高齢者と同程度の集積を示す症例も存在する．MCIが病理学的にはheterogeneousな集団であることを裏付ける所見といえる．また**図2**に示すように，MCI症例におけるBF-227の集積上昇は，AD患者に比べれば相対的に軽度である．このことからMCI段階では，老人斑の脳内蓄積はまだ進行途上にあることが示唆される．

4. ^{18}F標識プローブの開発状況

現在，PIBやBF-227などは半減期20分の

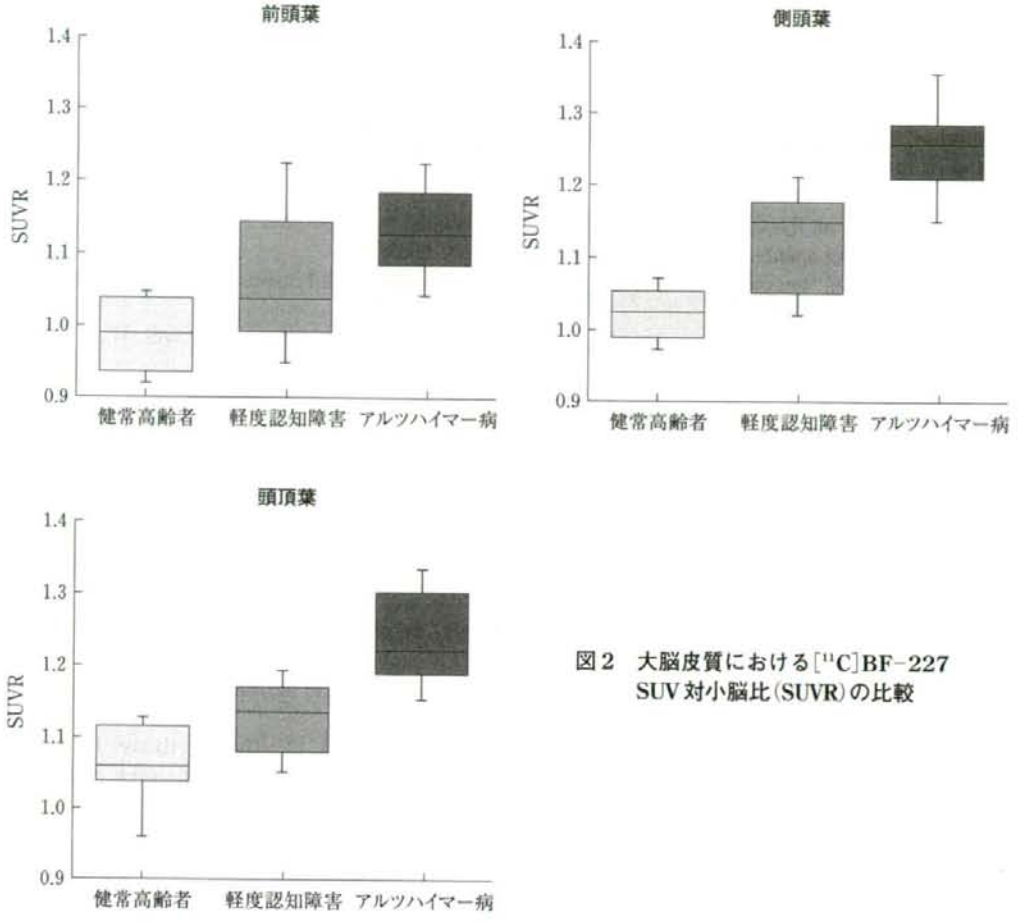

図2 大脳皮質における[^{11}C]BF-227 SUV対小脳比(SUVR)の比較

^{11}Cで標識されていることから，薬剤供給面での制約があり，検査実施可能な施設が限定されている．本検査の普及を図るには，放射性薬剤として供給できる^{18}F(半減期110分)で標識したPETプローブ，ないしはSPECT用に^{123}I(半減期13.2時間)で標識したプローブの実用化が望まれる．^{18}F標識プローブとしては，FDDNPが既に実用化されているが[14]，PIBなどと比べて，老人斑蓄積部位の非蓄積部位に対するコントラストが不良である．現在，PIB，SB-13の^{18}F標識体である[^{18}F]3′-F-PIB，[^{18}F]AV1の臨床評価が海外で進められており，良好な成績を収めている．著者らも新規^{18}F標識プローブの臨床評価へ向けて準備を進めており，PET診断用薬剤としての供給を目指している．

おわりに

アミロイドイメージング検査が広く普及すれば，今後多くの臨床施設で本検査が認知症の診断や治療評価のプロセスに組み込まれることになる．ただし，本検査が健常人のAD発症予測にどれほど信頼性の高い情報を提供できるのか，まだ十分なエビデンスが得られていない．今後，一般住民を対象とした大規模な長期フォローアップ研究を通じて，正常加齢と病的過程の線引きを行わねばならない．

■文　献

1) Chong MS, Sahadevan S: Preclinical Alzheimer's disease: diagnosis and prediction of progression. Lancet Neurol **4**: 576-579, 2005.
2) Price JL, Morris JC: Tangles and plaques in nondemented aging and "preclinical" Alzheimer's disease. Ann Neurol **45**: 358-368, 1999.
3) Cai L, et al: Radioligand development for PET imaging of β-amyloid (Aβ) —current status. Curr Med Chem **14**: 19-52, 2007.
4) Mathis CA, et al: Synthesis and evaluation of 11C-labeled 6-substituted 2-arylbenzothiazoles as amyloid imaging agents. J Med Chem **46**: 2740-2754, 2003.
5) Klunk WE, et al: Imaging brain amyloid in Alzheimer's disease with Pittsburgh Compound-B. Ann Neurol **55**: 306-319, 2004.
6) Rowe CC, et al: Imaging β-amyloid burden in aging and dementia. Neurology **68**: 1718-1725, 2007.
7) Lopresti BJ, et al: Simplified quantification of Pittsburgh Compound B amyloid imaging PET studies: a comparative analysis. J Nucl Med **46**: 1959-1972, 2005.
8) Klunk WE, et al: The binding of 2-(4'-methylaminophenyl) benzothiazole to postmortem brain homogenates is dominated by the amyloid component. J Neurosci **23**: 2086-2092, 2003.
9) Mintun MA, et al: [11C]PIB in a nondemented population: potential antecedent marker of Alzheimer disease. Neurology **67**: 446-452, 2006.
10) Fagan AM, et al: Inverse relation between in vivo amyloid imaging load and cerebrospinal fluid Aβ42 in humans. Ann Neurol **59**: 512-519, 2006.
11) Bacskai BJ, et al: Molecular imaging with Pittsburgh Compound B confirmed at autopsy: a case report. Arch Neurol **64**: 431-434, 2007.
12) Okamura N, et al: Styrylbenzoxazole derivatives for in vivo imaging of amyloid plaques in the brain. J Neurosci **24**: 2535-2541, 2004.
13) Kudo Y, et al: 2-(2-[2-Dimethylaminothiazol-5-yl]ethenyl)-6-(2-[fluoro]ethoxy) benzoxazole: a novel PET agent for in vivo detection of dense amyloid plaques in Alzheimer's disease patients. J Nucl Med **48**: 553-561, 2007.
14) Small GW, et al: PET of brain amyloid and tau in mild cognitive impairment. N Engl J Med **355**: 2652-2663, 2006.

臨床応用　脳の分子イメージング

アルツハイマー病

岡村信行[1]　古本祥三[2]　工藤幸司[2]　谷内一彦[1]

Alzheimer's disease

[1]Nobuyuki Okamura, [2]Shozo Furumoto, [2]Yukitsuka Kudo, [1]Kazuhiko Yanai
[1]Department of Pharmacology, Tohoku University Graduate School of Medicine
[2]Tohoku University Biomedical Engineering Research Organization (TUBERO)

Abstract

Progressive accumulation of amyloid plaques in the brain is a characteristic pathological change in Alzheimer's disease (AD) and precedes the presentation of cognitive impairment. *In vivo* detection of amyloid deposits using molecular imaging technique would thus prove useful for early diagnosis of AD and tracking disease progression. Several imaging agents have been developed that can noninvasively detect amyloid plaques in the brain and successfully differentiated AD patients from healthy normal individuals using positron emission tomography. Although validation remains required as to whether retention of these agents in the neocortex truly reflects the level of amyloid deposition, such findings suggest the potential usefulness of amyloid imaging technique for early diagnosis of AD.

Key words: Alzheimer's disease, amyloid-β protein, senile plaque, positron emission tomography (PET)

はじめに

我が国における認知症患者数は増加の一途をたどっており，患者数削減へ向けた取り組みが急務とされている．その最大の原因疾患であるアルツハイマー病(Alzheimer's disease: AD)の脳内では，アミロイドβ蛋白(amyloid-β protein: Aβ)の産生亢進，代謝・排泄の低下によって，その脳内濃度が上昇し，本来は可溶性であるAβが線維化して，脳内に蓄積する．このプロセスがADの病態に深く関与していると考えられている(アミロイド仮説)[1]．ADを特徴付ける脳病理変化は，Aβが細胞外に蓄積した凝集物である老人斑と，タウ蛋白が神経細胞内に蓄積して形成された神経原線維変化の沈着である．健常人の脳においても老人斑はしばしば観察されるが，一般に正常加齢に伴う老人斑の蓄積量やAβ線維化の程度は低く，ADとは大きな隔たりがある．

老人斑の脳内への蓄積は，ADの初期症状である物忘れ症状が現れるよりも数十年前に先行して出現する(**図1**)[2]．したがって，分子イメージングによってこれらの病理像を検出できれば，AD患者を病初期の段階で見いだすための理想的な診断法となり得る．このような背景から，老人斑を生体画像化する画像診断法は'アミロ

[1]東北大学大学院医学系研究科機能薬理学分野　[2]東北大学先進医工学研究機構高度情報通信分野

0047-1852/07/¥40/頁/JCLS

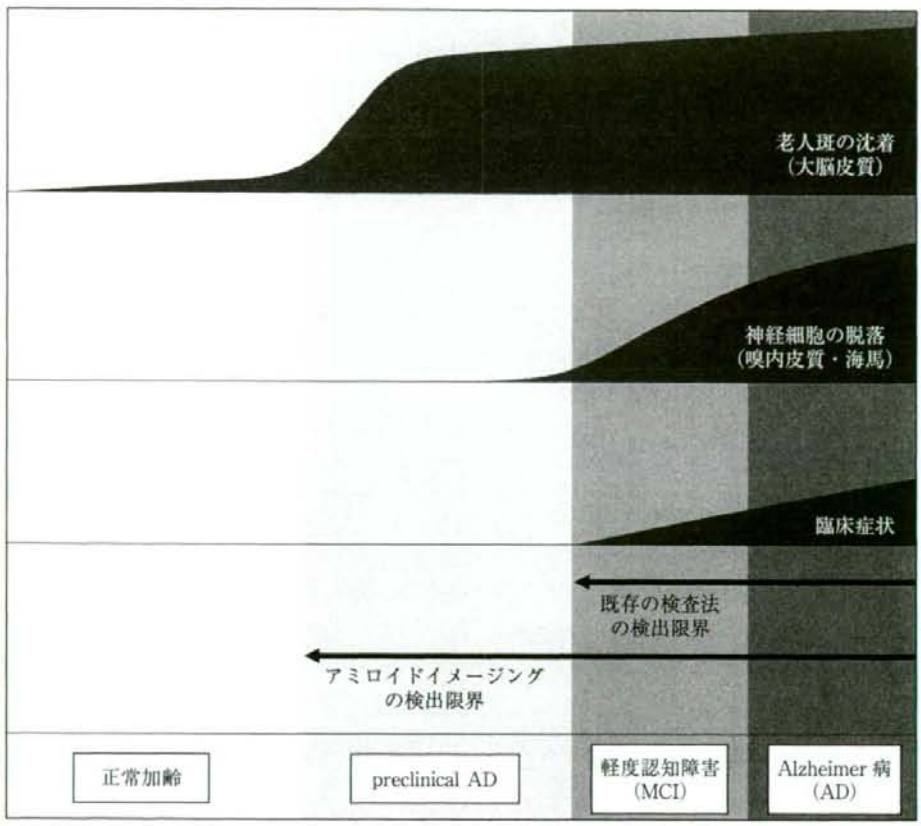

図1 アルツハイマー病における病理像と臨床像の関係

イドイメージング'という名前で近年注目を浴びるようになった.

本稿では, AD診療分野における分子イメージングの代表的な応用例として, アミロイドイメージングに焦点を当てて概説する.

1. アミロイドイメージングの有用性とは

アミロイドイメージングでは, 老人斑の蓄積という疾患特異性の高い病変を指標とすることから, 従来の検査法よりも高精度にADの早期診断を可能にする. もちろん有効な治療法がなければ早期診断を行う意義は薄いのであるが, 近年, 免疫療法やβ・γセクレターゼ阻害薬といったADの進行を抑止する根本的治療法の開発が進められている[3]. 今後, こうした根本的治療薬が利用可能となれば, 可能なかぎり早期, できれば神経細胞へのダメージが少ない発症前段階でADを診断して, 治療を開始することが求められるようになる. また副作用のリスクが懸念される治療においては, 治療対象となるべき症例を適切に選択する必要も生ずる. このような要請に応えられる検査法は, 現状ではアミロイドイメージング以外には考えられない. またAβの蓄積抑制を目標とした治療, 特にワクチン療法のように線維化したAβの劇的な減少が期待されるような治療においては, その薬効評価系としての活用も期待できる.

2. アミロイドイメージング用プローブの開発と臨床応用

現状において, アミロイドの分子イメージングに最も適した方法は, PET/SPECTを用いた核医学的手法である. 老人斑を構成する線維化したAβは, βシート構造と呼ばれる二次構造

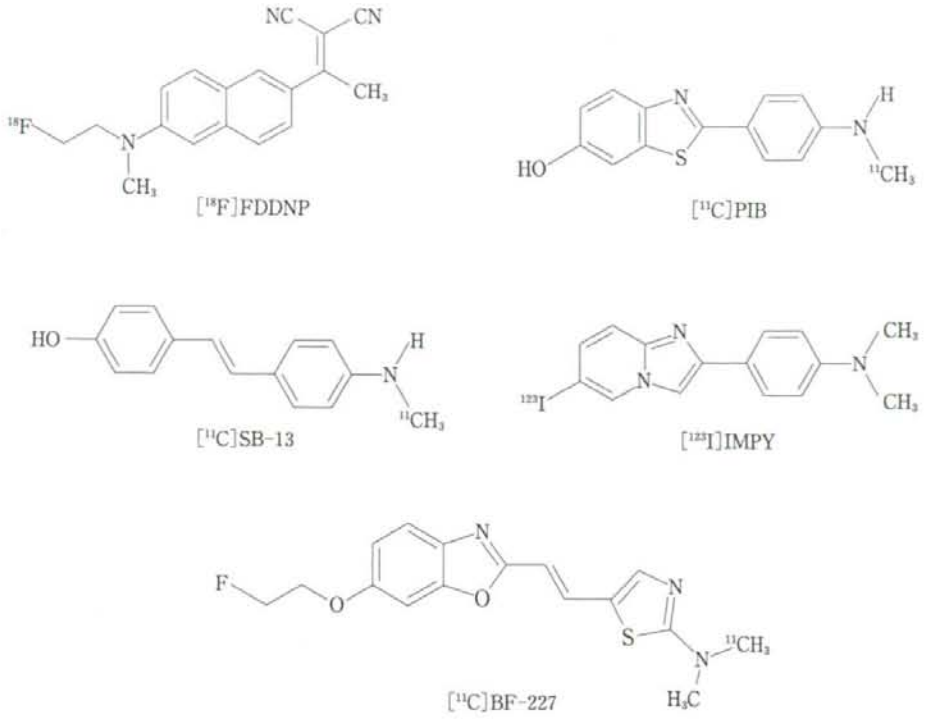

図2 主なアミロイドイメージング用プローブの化学構造式

を形成する．Congo-redやThioflavin-Tのように従来から試薬として使われてきた化合物の中には，βシート構造に高い結合親和性を有するものが数多く存在する．そこで，このような化合物をもとにして，線維化Aβに対する結合親和性，脳血液関門(BBB)透過性，正常組織からのクリアランスなどの特性のバランスを考慮した構造最適化が行われ，様々なプローブが開発された．これまでのところ，FDDNP，PIB，SB-13，IMPY，BF-227の5化合物がアミロイドイメージング用プローブとして臨床応用されている(**図2**)．

a. [18F]FDDNP

FDDNPは，アミノナフタレン骨格を有する^{18}F標識用化合物であり，米国UCLAの研究グループによって開発された．アミロイドイメージング用プローブとして世界で初めて臨床応用された化合物であり，ADの二大病理像である老人斑，神経原線維変化の両者に対する結合性を有する[4]．AD患者を対象に施行されたPET studyでは大脳皮質および海馬領域での集積上昇が観察され，健常者とは異なる集積像を示す．このことから，FDDNP-PETにおける集積像は，老人斑・神経原線維変化の両者との結合を反映していると考えられる[5]．FDDNPは^{18}F標識プローブとして唯一使用可能な薬剤であり，AD早期診断への活用が期待される．ただし，脂溶性の高さに起因するとみられる白質や脳幹部への非特異的集積が目立ち，特異的集積部位とのコントラストが不良であることが問題点として指摘されている．

b. [11C]PIB

Thioflavin-Tのイオン性電荷を取り除き，適度な脂溶性をもつように最適化されて誕生したのが6OH-BTA-1であり，米国ピッツバーグ大学で開発されたことからPittsburgh compound B(PIB)と命名された[6,7]．PIBの^{11}C標識体は，既に多くの施設でAD診断における有用性が確認され，また定量法も確立されている[8-10]．AD患者のPIB-PET画像では，老人斑の好発部位で

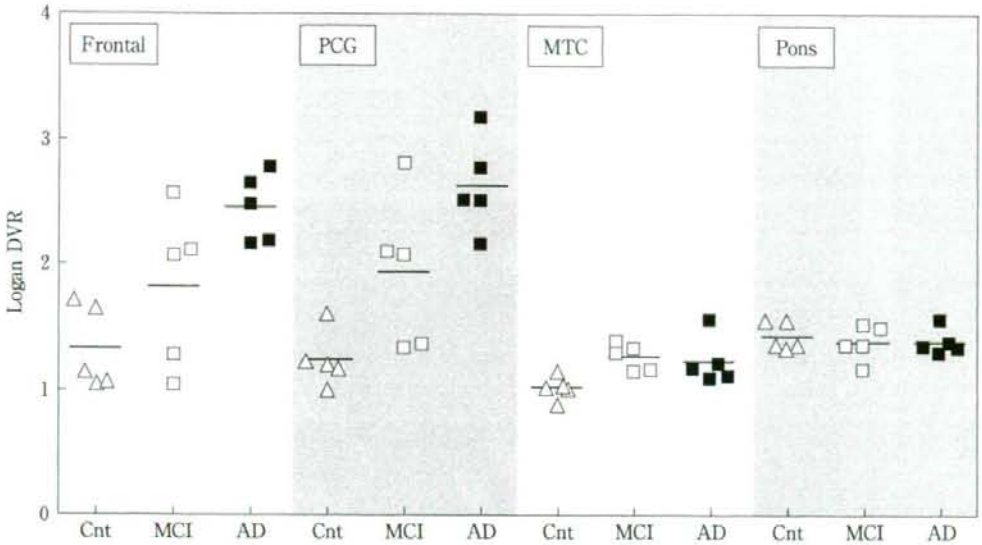

図3 [^{11}C]PIB-PETで計測されたLogan-DVR値(文献[9]より改変)
Cnt: 正常対照, MCI: 軽度認知障害, AD: アルツハイマー病, Frontal: 前頭葉, PCG: 後部帯状回, MTC: 内側側頭葉, Pons: 橋.

ある大脳皮質において顕著なプローブの集積を認める. 老人斑の沈着しない大脳白質や脳幹部においても軽度の集積を認めるが, AD患者と健常者の集積レベルに差がないことから, ミエリンへの吸着を反映した非特異的な集積と考えられる(**図3**). 一方, 神経原線維変化の好発部位である内側側頭葉領域では, AD患者においても集積上昇を認めない. このことからPIBは老人斑への結合選択性の高いプローブと考えられる. PIBの大脳皮質における集積量は, FDG-PETにより計測された糖代謝率と負の相関を示す[8]. また, PIBの集積量とFDG-PETで計測された糖代謝率を健常者群とAD患者群間で比較した場合, PIB-PETの方が群間でのオーバーラップが少ない. このことから, PIB-PETはFDG-PETよりもAD早期診断における鑑別精度に優れていることが示唆される.

早期あるいは発症前の段階で, 将来のADへの進行をPIB-PETで予測できるか否かに関しては, まだ十分なエビデンスが得られていない. ADの発症予備群とされている軽度認知障害(MCI)の症例におけるPET studyでは, AD患者と同様に高い集積を示す症例と, 健常者と同レベルの症例に二分される[9,10]. この結果の解釈として, 前者は既にADの病理像を呈しADへの進行が避けられないMCI症例, 後者はADとは異なる病態に基づく非進行性のMCIである可能性が想定されるが, その真偽については今後のフォローアップ研究を待たねばならない. では, MCIより前の無症候段階で, PIB-PETを用いたADの診断は本当に可能であろうか? 最近発表された健常人を対象としたPIB-PET study[11]では, 41人中4人の健常人がAD患者と同様の高い集積値を示していた. また脳脊髄液マーカーを含めた検討[12]において, PIB-PETで大脳皮質に高い集積を認め, かつ脳脊髄液中Aβ42濃度がAD患者と同レベルに低下した3人の健常高齢者の存在が報告されている. 彼らは, 無症候ながらも脳内に老人斑の多数蓄積したAD発症予備段階の症例(preclinical AD, **図1**)であるかもしれない. 同症例が今後ADを発症するか否か, 興味のもたれるところである.

c. [^{11}C]SB-13

米国ペンシルバニア大学グループによって開発されたスチルベン骨格を有する^{11}C標識用化合物である[13]. [^{11}C]SB-13の臨床評価は, [^{11}C]PIB